International Journal on Advanced Science Engineering Information Technology

Vol.12 (2022) No. 1
ISSN: 2088-5334

Evaluation of Parameter Selection in the Bivariate Statistical-based Landslide Susceptibility Modeling (Case Study: the Citarik Sub-watershed, Indonesia)

Sukristiyanti [a,b,*], Ketut Wikantika [a,c], Imam Achmad Sadisun [d], Lissa Fajri Yayusman [c], Adrin Tohari [b], Moch. Hilmi Zaenal Putra [b,d]

[a] *Remote Sensing and GIS Research Group, Faculty of Earth Sciences and Technology, Bandung Institute of Technology (ITB), Indonesia*
[b] *Research Center for Geotechnology, National Research and Innovation Agency (BRIN), Bandung, Indonesia*
[c] *Center for Remote Sensing, Bandung Institute of Technology (ITB), Indonesia*
[d] *Applied Geology Research Group, Faculty of Earth Sciences and Technology, Bandung Institute of Technology (ITB), Indonesia*
Corresponding author: [*]sukris.tiyanti@gmail.com; sukristiyanti@brin.go.id

***Abstract*— A landslide susceptibility mapping is essential for landslide hazard mitigation to reduce the associated risk. This paper aims to present the results of the landslide susceptibility modeling in the Citarik sub-watershed using three bivariate statistical-based methods, i.e., frequency ratio (FR), information value (IV), and weight of evidence (WoE). The main objective of this study is to evaluate the significance of the threshold of the area under curve (AUC) value in parameter selection. In this study, 118 landslide pixels were compiled from Google Earth images, unmanned aircraft vehicle (UAV) aerial photos taken just after the landslide, official landslide reports, and field observation. Thirteen landslide causative factors were prepared in Geographic Information System (GIS) environment, derived from various satellite images and maps. The landslide data were divided into two groups, 70% of data as training data and the rest as test data. Two scenarios that involve a different number of parameters were compared to explain the threshold of the AUC value in parameter selection and model accuracy. The result of this study shows that the AUC value threshold of 0.6 for parameter selection cannot be applied in all cases, and the performance of both two scenarios was excellent in assessing landslide susceptibility in this study area. Those three landslide susceptibility zonation maps of the best scenario showed that the sub-watershed's northern, northeastern, south-eastern, and southern parts were under high to very high susceptibility to landslides, including the Cimanggung area where a recent deadly double landslide occurred.**

***Keywords*— Bivariate statistical-based method; GIS; landslide susceptibility mapping; modeling.**

Manuscript received 19 Mar. 2021; revised 2 Aug. 2021; accepted 13 Sep. 2021. Date of publication 28 Feb. 2022.

I. INTRODUCTION

A devastating double landslide occurred in the village of Cihanjuang in Cimanggung District, Sumedang Regency, West Java Province, Indonesia, in January 9, 2021 [1]. The National Disaster Management Agency (BNPB) reported that the landslide caused 40 people dead. The first slope failure occurred at 4 pm (GMT+07:00). The subsequent landslide hit the same site about three hours later while some rescue personnel evacuated the victims. Fig. 1 shows the aerial photo of post-disaster conditions taken by the unmanned aircraft vehicle (UAV) a week after the landslide.

As shown in Fig. 1, the landslide area can be classified into three parts, i.e., source area, flow tracking, and depositional area. Although most of the flow track is an unbuilt-up area, the run-out zone is located with a settlement area. Therefore, the landslide caused many casualties. In addition, the landslide also caused damages to some houses located in the main landslide scarp.

The 2021 deadly double landslide should increase awareness of the dangers of landslides. Therefore, this study aims to generate a landslide susceptibility map for the Citarik sub-watershed, a location where the deadly landslide occurred. The landslide susceptibility mapping (LSM) is an initial effort to mitigate landslide hazards [2], [3]. This mapping is on a medium scale in which there are two widely used models, i.e., expert-driven and data-driven models, while the physical and deterministic models are the most suitable for a single landslide large-scale mapping [4], [5]. Therefore, to avoid

subjectivity aspects as much as possible in the medium-scale mapping, data-driven was used in this research [6], [7].

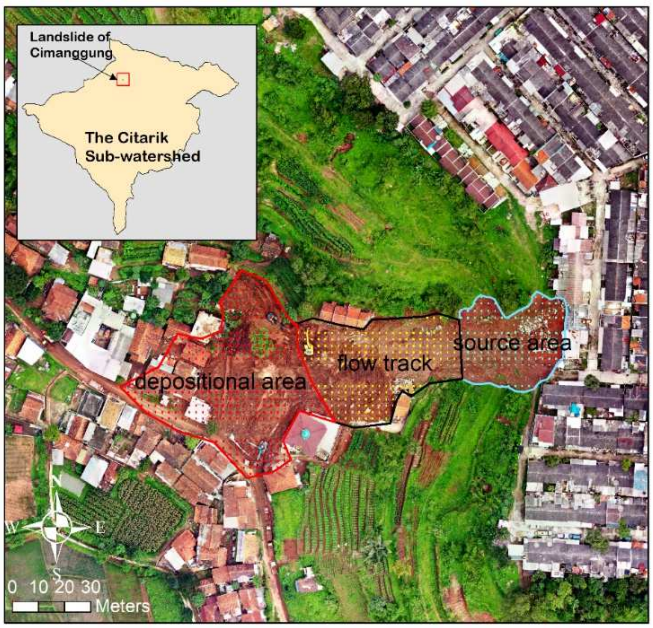

Fig. 1 The post-deadly landslide condition on the unmanned aircraft vehicle (UAV) aerial photos

Two methods, namely statistical- and machine learning-based models, have been extensively used for LSM. Those methods were more frequently used and developed due to the increasing availability of remote sensing data as the main contributor to landslide inventory data supported by information technology developments [8]–[11].

Frequency ratio [7], [12]–[14], information value [12], [15], [16], and the weight of evidence [17]–[20] are some bivariate statistics-based methods. Meanwhile, logistic regression [13], [21]–[23] and probit regression [17] are multivariate statistics-based methods. Besides, the methods based on machine learning are abundant and highly developed recently, e.g., artificial neural network [21], [24], decision tree [25], [26], support vector machine [27], and random forest [25], [28], [29]. However, no method is extraordinary and highly recommended because of its accuracy level [20], [30]. Therefore, many researchers used any methods to generate landslide susceptibility mapping [13], [25].

This paper aims to demonstrate the application of three bivariate statistical-based methods, i.e., frequency ratio (FR), information value (IV), and weight of evidence (WoE) for landslide susceptibility mapping in the Citarik sub-watershed area where the 2021 deadline double landslide occurred. The selected statistical methods are considered straightforward [22] and can be executed easily within a Geographic Information System (GIS) environment. While some previous studies have focused on a comparative study of those three methods using a point-based landslide inventory map [15], [31], this current study used the polygon-based inventory map because it is more representative than the point-based one [20], [32], [33].

Some previous studies on the bivariate statistical-based modeling used a parameter selection [6], [15], [18], [19], [34]–[36] and among others did not [37]. Parameter selection is an important step in removing insignificant parameters, making modeling more efficient and accurate [18]; therefore, this study was designed to apply parameter selection. The use of the threshold of the area under curve (AUC) value for landslide parameter selection was used by some previous studies [19], [34], [36]. They inferred that AUC values less than 0.6 were poor in predicting landslide occurrence, referring to the AUC value classification stated by a previous study [38]. In other words, a parameter with an AUC value less than 0.6 shows that there is no adequate spatial relationship between the related parameter and the landslide occurrences. They did not involve parameters with the AUC value less than 0.6 in the modeling [19], [34], even parameters with the AUC values slightly above 0.6, i.e., distance to the river and land cover with the AUC values of 0.612 and 0.606, respectively [36].

The use of the AUC value threshold in parameter selection is interesting, but it leaves a question, whether the threshold value of 0.6 is requisite or not. Therefore, the main objective of this current study was to investigate the effect of the AUC value threshold of 0.6 in landslide parameter selection for accurate modeling with bivariate statistical methods.

II. Material and Method

A. Study Area

The Citarik sub-watershed was chosen as this study area. It has an area of 268.66 sq km. It is a sub-watershed of Bandung Basin, located in the eastern part of the basin. The study area is located at 107.70°–107.95°E and 6.91°–7.13°S, including some sub-districts, e.g., Cimanggung, Rancaekek, Cicalengka, Nagrek, Cikancung, and Majalaya. Mt. Guntur borders the sub-watershed in the south and Mt. Kerenceng in the north (Fig. 2).

The area's altitude ranges from 657 to 1,917 m above the mean sea level. The slopes vary from 0° to 54° or 0% to 138%. The study area consists of several geomorphology units. The rough terrain is dominated by volcanic forms, e.g., an ancient volcanic cone, a parasitic young volcanic cone, and a young volcanic cone. Meanwhile, the geomorphological unit in the flat area is the *fluvio* lacustrine plain. In the study area, volcanic products dominate lithological units at high altitudes, and lake deposits are found at lower altitudes. This study area's average annual rainfall (2010 – 2019) gradually increased from the southern part to the northern part. In the period, the site of 2021 deadly landslide had a high rainfall.

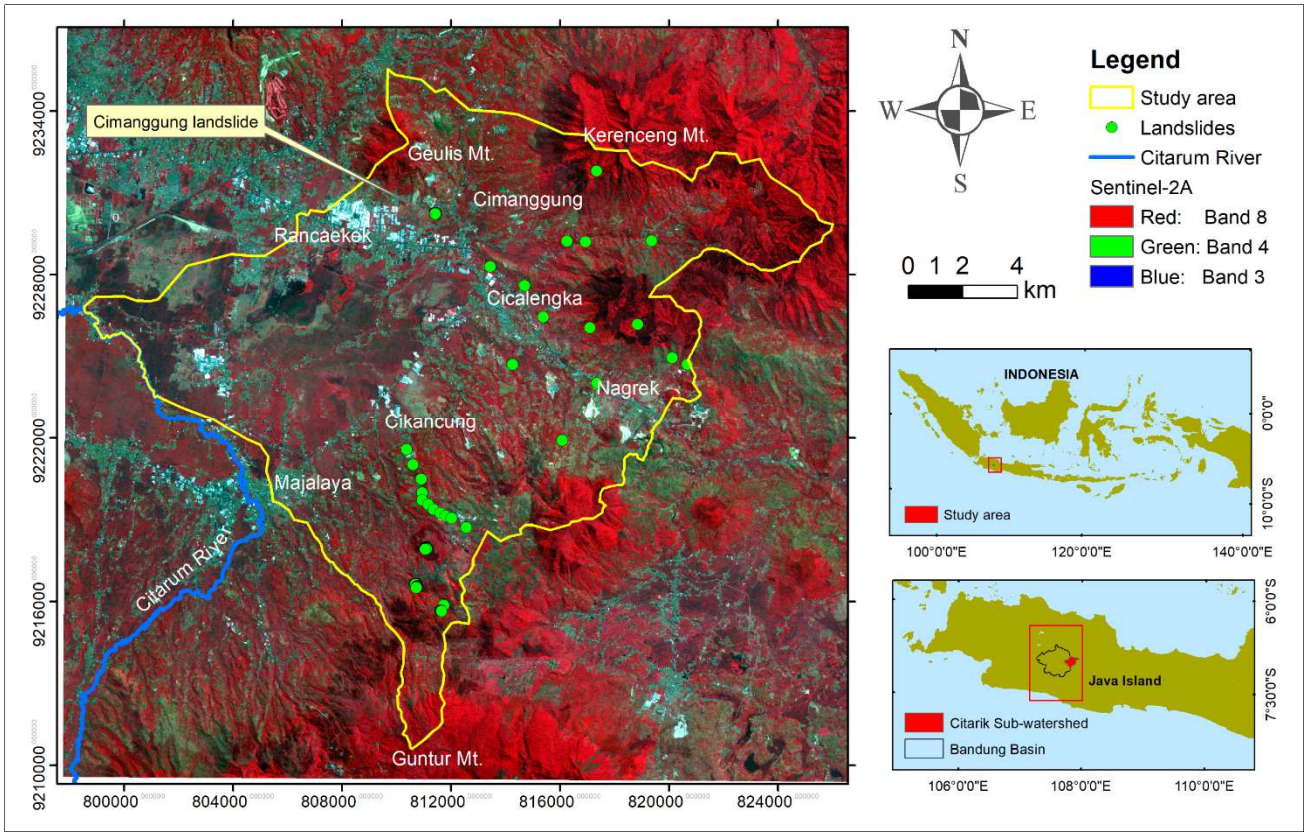

Fig. 2 The map of the study area (the Citarik sub-watershed)

B. Data and Research Methodology

The Geospatial database for this landslide susceptibility mapping (LSM) study involved a polygon and point-based landslide inventory data and thirteen landslide causative factors, i.e., elevation, slope (%), aspect, slope curvature, distance to rivers, river density, lithology, geomorphology, peak ground acceleration (PGA), rainfall, distance to roads, road density, and vegetation index (NDVI: normalized difference vegetation index). The inventory map consisted of old landslides and landslides that just happened in Cimanggung, Sumedang. The landslide inventory is a fundamental step to assess landslide susceptibility, which contains information about the location and timing of landslides [14], [39].

The inventory map was compiled from UAV (unmanned aircraft vehicle) aerial photos and a time series of Google Earth imageries, supported by an official landslide report and a field survey. The mix of polygons and points because of the difference in the size of the landslides. Small landslides which were unrecognized in the imageries were represented as points. The inventory map in this study represents the source area of landslides [40]. Similar to landslide causative factors, the landslide inventory map was also prepared as a raster map with a pixel size of 8.35, referred to as the pixel size of the used DEM (data elevation model). The total of landslide pixels was 118 pixels, in which 24 landslide pixels were derived from landslide points, and 94 landslide pixels were converted from landslide polygons. For LSM modeling, 70% (83 pixels) of the landslide pixels was used as modeling, and the rest (35 pixels) was used for validation. This ratio was most widely applied in previous LSM studies [11], [39], [41].

Various sources of data were used for deriving landslide causative factors. The topographical map from the Geospatial Information Agency with a map scale of 1:25,000 was used to obtain some parameters: distance to roads, distance to rivers, road density, and river density. The geological and geomorphological maps published from Geological Agency were used to obtain lithological and geomorphological maps. The peak ground acceleration (PGA) map published by Geological Agency was used here. The digital elevation model, namely DEMNAS (Seamless digital elevation model and National bathymetry) with a pixel size of 8.35, was used to derive elevation or altitude, slope, aspect, and slope curvature parameters.

Similar to [10], NDVI was extracted from Sentinel-2 satellite imagery (provided by the European Space Agency). Two bands of Sentinel-2: band-8 representing the Near-Infra Red (NIR) band and band-4 representing the Red band, acquired in 2019, were used to obtain NDVI in this study. Regarding the rainfall variable, it was derived from PERSIANN-CCS (Precipitation Estimation from Remotely Sensed Information using Artificial Neural Networks - Cloud Classification System), which is a real-time global high resolution (4km x 4km) satellite precipitation product developed by the Center for Hydrometeorology and Remote Sensing (CHRS) at the University of California (UCI). Similar to [22], [42], this study used mean annual rainfall data to describe rainfall patterns across the study. The 2010-2019 average annual rainfall per pixel from the PERSIANN-CCS data was interpolated using the Kriging interpolation method.

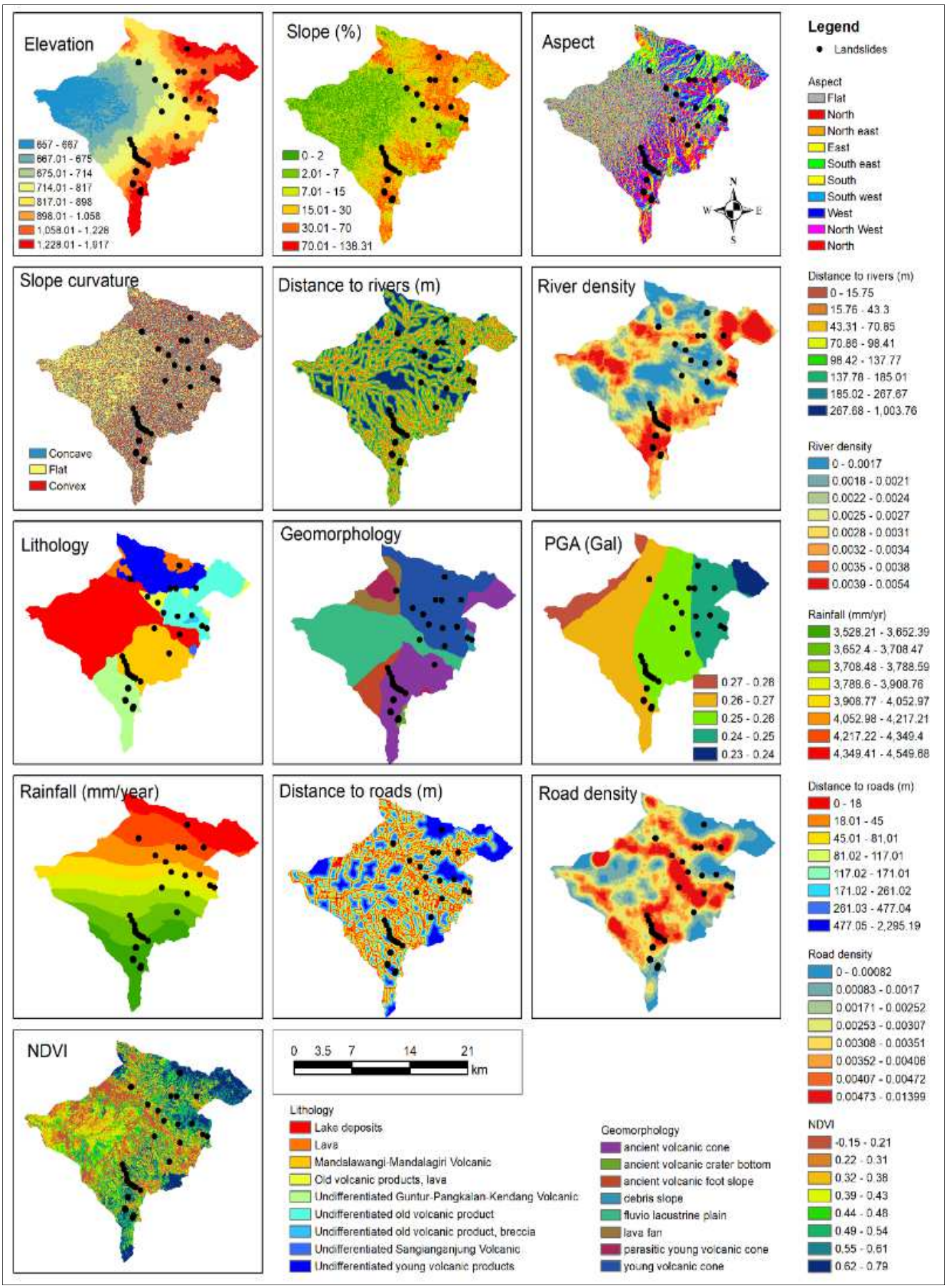

Fig. 3 Maps of landslide causative parameters for the study area

Most of these variables are continuous data, and the rest are categorical data, i.e., lithology, geomorphology, and PGA. Since the bivariate statistical analysis requires categorical data, it is necessary to classify the continuous data. Therefore, some of the continuous data were classified. The manual classification method was applied to the slope (%), aspect, slope curvature variables. The slope (%) data were classified using Van Zuidam's classification into seven classes [43]. The aspect data were classified into ten classes, and the curvature was classified into three classes, i.e., flat, concave, and convex. Some previous studies used such a curvature classification [6], [7], [35], [37]. Meanwhile, the quantile classification method was applied to the rest, i.e., elevation, distance to rivers, river density, rainfall, distance to roads, road density, and vegetation index (NDVI). All classified parameter maps can be seen in Fig. 3.

Three bivariate statistical-based methods, namely frequency ratio (FR), information value (IV), and weight of evidence (WoE), were used for mapping the landslide susceptibility of the Citarik sub-watershed. Frequency ratio (FR) is the most simple and popular bivariate statistical-based method for LSM. It calculates the ratio between landslide density in each class with landslide density in the study area [7], [12]–[14]. The information value (IV) model is a product of a natural log of FR, which is similar to the statistical index (SI) model [12], [15], [44].

WoE is a bivariate statistical method based on the Bayesian probability model based on evidence. It has been used to model mineral potency and adopted for landslide susceptibility modelling [45]. Positive weights or true-positive (W^+) and negative weights or true negative (W^-) are used to assess susceptibility. W^+ is a location predicted as a susceptible area, and that is true. Conversely, W^- is a location predicted as a safe area from a landslide, and that is true. The algorithms for obtaining WoE are given in equations 1-3 [19], [45].

$$W^+ = \ln\left(\frac{A/B}{C/D}\right) \quad (1)$$

$$W^- = \ln\left(\frac{E/B}{F/D}\right) \quad (2)$$

$$WoE = W^+ - W^- + \sum W^- \quad (3)$$

where:
W^+ = true-positive, W^- = true-negative
ΣW^- = total of W^-
A = landslide pixels in an observed class
B = landslide pixels in the study area
C = non-landslide pixels in an observed class
D = non-landslide pixels in the study area
E = landslide pixels outside of the observed class
F = non-landslide pixels outside of the observed class

Frequency ratio (FR), information value (IV), and weight of evidence (WoE) methods were performed to assign the weight for each class of all involved parameters [15], [19], [20]. It represents the level of landslide probability [6], [7]. The landslide susceptibility map of FR, IV, or WoE is represented as an index map, namely landslide susceptibility index (LSI), derived from the sum of the related weights of all the factors involved, as shown in equation 4 [6]. The weight is the probabilistic value of each method of all used thematic layers (n). LSI varies from the lowest to the highest values representing the probability of landslides, the higher the value, the higher the probability of landslides.

$$LSI = \sum_{i=1}^{n} \text{the weight} \quad (4)$$

In this study, the receiver operating characteristics (ROC) curve analysis was conducted to assess (1) the level of significance of each parameter in controlling landslide [19], [34], [36] and (2) the validation of the models [2], [28], [46]. ROC curve analysis yields the curve and the area under curve (AUC) value. The ROC curve is a graphical plot that shows the false positive values (1-specificity) in the X-axis and the true positive values (sensitivity) in the Y-axis. The AUC values vary between 0.5 (random assignment) and 1 (ideal prediction) [15], [29], [37], [47], [48]. In more detail, the AUC value can be classified into five classes, i.e., 0.5 – 0.6 (bad), 0.6 – 0.7 (moderate), 0.7 – 0.8 (good), 0.8 – 0.9 (very good), and 0.9 – 1 (excellent) [38], [49]. The true positive values (Y-axis) are obtained from the cumulative landslide occurrence (in %). Meanwhile, the false-positive values (X-axis) were obtained from the cumulative weight rank of a related factor (in %) for validating landslide causative factors or were obtained from the cumulative LSI rank (in %) for validating the landslide susceptibility models [48]. The formula of AUC is defined in equation 5 [19], [45].

$$AUC = \sum_{i=0}^{n}(x_i - x_{i-1})y_i - \left[\frac{(x_i - x_{i-1})(y_i - y_{i-1})}{2}\right] \quad (5)$$

where:
x_i = percentage of area, y_i = percentage of landslide area

The AUC values of landslide causative factors were used for parameter selection. Parameter selection is a step that should be taken before modeling is conducted for more efficient and accurate modeling [6]. Some previous studies used the AUC value of 0.6 as a threshold value in the parameter selection; in other words, parameters with an AUC value less than 0.6 are not involved in modeling [19], [34], [36]. In this study, two modeling scenarios that involve a different number of parameters were performed to evaluate the use of the AUC threshold value of 0.6. The methodology of this study can be summarized in the following flow chart (Fig. 4).

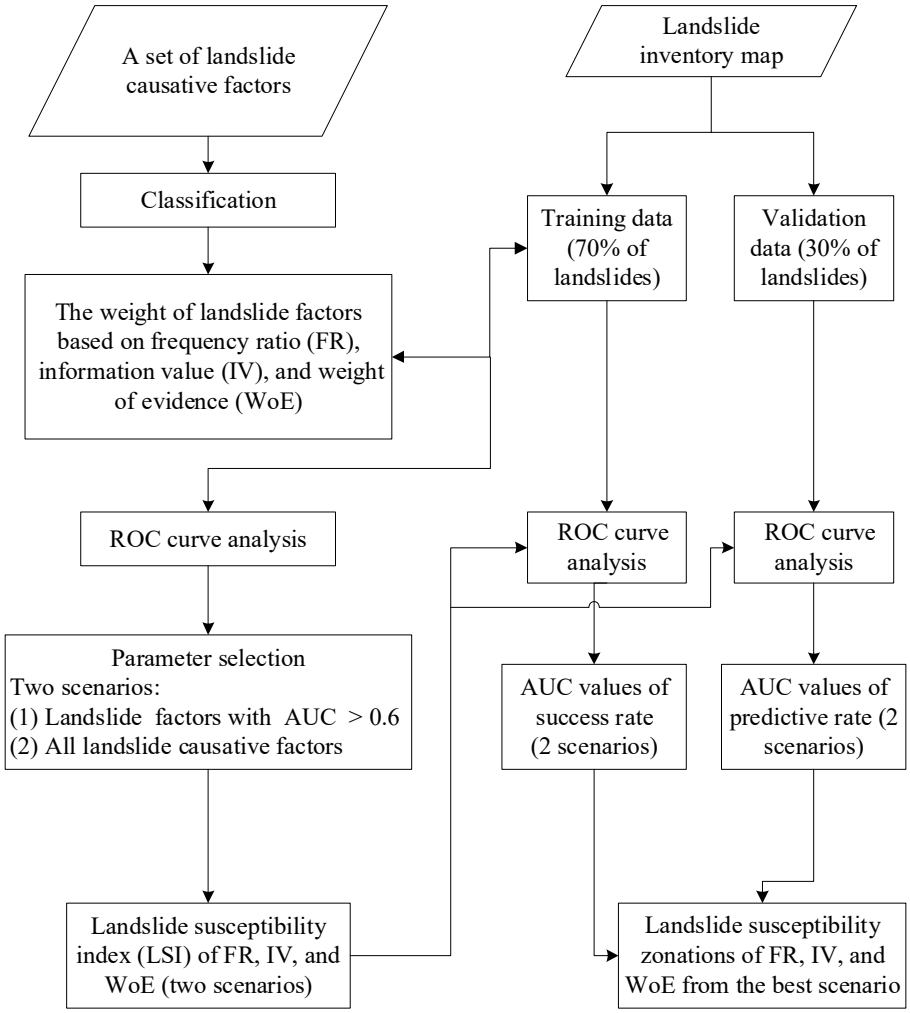

Fig. 4 Flow chart of the research methodology

III. Result and Discussion

Three bivariate statistical methods, namely frequency ratio (FR), information value (IV), and weight of evidence (WoE), were applied to evaluate landslide susceptibility in this study area. Each class of all parameters was assigned with the weight based on the three methods, representing their related probability to landslides. TABLE I presents the spatial relationship between landslides and thirteen landslide causative factors. From this table, the elevation class of 1,058.01 - 1,228 m has the highest FR value of 4.290. The value significantly stands out compared to other classes. The FR value of higher than 1 indicates that the class has a high probability of landslides [6]. The low-elevation ranges of the study area have the lowest probability of landslides, i.e., classes of 657 - 667 m and 667.01 - 675 m with the same FR value of 0.012. Similar to FR, the highest probability of landslide using IV and WoE occurred in the elevation class ranging from 1,058.01 to 1,228 m above sea level.

For the slope factor, the highest value of FR is the steepest slope, i.e., class of 70.01 - 138.31 % (35 - 54.13°). The slope class above 35° has the highest landslide probability for the IV model, but it is different for WoE. The highest probability of landslides according to the WoE model occurs in the range of 30.01 - 70 % (16.7 – 35°). Four classes of gentle slopes have a low probability of landslides with values of less than zero. Many previous studies also showed that the gentle slopes were associated with low FR values because they have less shear stress [6], [7], [15], [50].

The models show that the southwest-facing slopes have the highest probability of landslides in the slope aspect parameter, with the FR, IV, and WoE values being 2.907, 1.067, and 1.323, respectively. Conversely, north-facing slopes have the lowest probability for all those models, as shown by the FR value of less than 1, even close to zero. In contrast, the values of IV and WoE for the north-facing slopes are negative, as shown in TABLE I. Similar interpretations for other landslide causative factors can be made from all weight values shown in TABLE I.

TABLE I
The spatial relationship between landslides and the 13 causative factors by using FR, IV, and WoE

Parameters	Σ pixels	Σ landslide pixels	FR	IV	WoE
Elevation (m)					
657 – 667	553005	0	0.012	-4.431	-4.771
667.01 – 675	474351	0	0.012	-4.431	-4.748
675.01 – 714	473089	1	0.109	-2.217	-2.521
714.01 – 817	473049	16	1.565	0.448	0.343
817.01 – 898	472417	4	0.401	-0.915	-1.182
898.01 – 1.058	471509	7	0.694	-0.366	-0.595
1,058.01 – 1,228	472213	44	4.290	1.456	1.884

1,228.01 – 1,917	467163	11	1.093	0.089	-0.085
Slope (%)					
0 – 2	590097	0	0.012	-4.431	-5.662
2.01 – 7	707583	0	0.012	-4.431	-5.698
7.01 – 15	789680	0	0.012	-4.431	-5.724
15.01 – 30	951645	6	0.301	-1.199	-2.472
30.01 – 70	787823	73	4.266	1.451	2.207
70.01 – 138.31	29968	4	6.140	1.815	0.789
Aspect					
Flat (-1)	719954	1	0.076	-2.581	-2.873
North (0°to 22.5°)	172494	0	0.012	-4.431	-4.576
North east (22.5° to 67.5°)	361726	2	0.266	-1.325	-1.498
East (67.5° to 112.5°)	222725	5	1.043	0.042	-0.055
South east (112.5° to 157.5°)	272623	7	1.191	0.175	0.090
South (157.5° to 202.5°)	398105	21	2.434	0.889	0.970
South west (202.5° to 247.5°)	523428	33	2.907	1.067	1.323
West (247.5° to 292.5°)	463535	13	1.300	0.262	0.204
North West (292.5° to 337.5°)	525338	1	0.099	-2.310	-2.542
North (337.5° to 360°)	196868	0	0.012	-4.431	-4.582
Distance to rivers (m)					
0.00 – 15.75	327156	7	0.994	-0.006	-0.098
15.76 – 43.3	634056	8	0.591	-0.526	-0.694
43.31 – 70.85	500012	2	0.196	-1.632	-1.836
70.86 – 98.41	461626	1	0.111	-2.195	-2.400
98.42 – 137.77	548263	4	0.347	-1.059	-1.253
137.78 – 185.01	475206	35	3.394	1.222	1.541
185.02 – 267.67	468619	15	1.482	0.393	0.371
267.68 – 1,003.76	441858	11	1.155	0.144	0.073
River density					
0.0000 – 0.0017	480313	2	0.203	-1.594	-1.844
0.0018 – 0.0021	491593	7	0.666	-0.407	-0.597
0.0022 – 0.0024	486002	12	1.146	0.136	0.014
0.0025 – 0.0027	476855	2	0.204	-1.587	-1.836
0.0028 – 0.0031	502344	4	0.378	-0.974	-1.206
0.0032 – 0.0034	482495	11	1.059	0.057	-0.077
0.0035 – 0.0038	468372	4	0.404	-0.906	-1.128
0.0039 – 0.0054	468822	41	4.027	1.393	1.793
Lithology					
Lake deposits	1505257	1	0.042	-3.160	-3.811
Lava	131889	4	1.404	0.340	0.182
Old volcanic products, lava	97459	2	0.954	-0.047	-0.221
Undifferentiated young volcanic products	516787	13	1.167	0.154	0.008
Undifferentiated Guntur-Pangkalan-Kendang Volcanic	406095	49	5.552	1.714	2.309
Undifferentiated Sangianganjung Volcanic	14242	0	0.012	-4.431	-4.607
Mandalawangi-Mandalagiri Volcanic	631339	11	0.812	-0.208	-0.417
Undifferentiated old volcanic product	538226	3	0.268	-1.317	-1.602
Undifferentiated old volcanic product, breccia	15502	0	0.012	-4.431	-4.607
Geomorphology					
Fluvio lacustrine plain	1214886	1	0.050	-2.990	-3.542
Parasitic young volcanic cone	136807	2	0.691	-0.369	-0.570
Lava fan	205428	10	2.274	0.822	0.706
Ancient volcanic crater bottom	23045	9	18.159	2.899	2.819
Ancient volcanic cone	908475	49	2.518	0.924	1.365
Debris slope	32188	0	0.012	-4.419	-4.617
Young volcanic cone	1129199	11	0.465	-0.766	-1.156
Ancient volcanic foot slope	206768	1	0.237	-1.441	-1.673
PGA (Gal)					
0.27 – 0.28	281275	0	0.012	-4.431	-4.627
0.26 – 0.27	1435263	42	1.355	0.304	0.419
0.25 – 0.26	1313012	33	1.166	0.153	0.121
0.24 – 0.25	667468	8	0.562	-0.576	-0.785
0.23 – 0.24	159778	0	0.012	-4.431	-4.594
Rainfall (mm/year)					
3,528.21 – 3,652.39	478457	50	4.810	1.571	2.080
3,652.4 – 3,708.47	490140	8	0.761	-0.273	-0.573
3,708.48 – 3,788.59	495365	2	0.197	-1.623	-2.001
3,788.6 – 3,908.76	480558	1	0.107	-2.231	-2.617
3,908.77 – 4,052.97	488760	1	0.106	-2.246	-2.634
4,052.98 – 4,217.21	476838	3	0.301	-1.201	-1.562
4,217.22 – 4,349.4	475454	14	1.364	0.310	0.096
4,349.41 – 4,549.68	471224	4	0.402	-0.912	-1.259
Road density					
0.00000 – 0.00082	471810	4	0.401	-0.913	-1.043
0.00083 – 0.0017	473651	9	0.884	-0.123	-0.188
0.00171 – 0.00252	476044	13	1.266	0.236	0.225
0.00253 – 0.00307	484437	22	2.097	0.741	0.863
0.00308 – 0.00351	477297	0	0.012	-4.431	-4.610
0.00352 – 0.00406	524879	3	0.274	-1.293	-1.451
0.00407 – 0.00472	482570	23	2.200	0.789	0.928
0.00473 – 0.01399	466108	9	0.898	-0.107	-0.170
NDVI					
-0.15 – 0.21	470183	8	0.793	-0.232	-0.279
0.22 – 0.31	483236	3	0.297	-1.214	-1.329
0.32 – 0.38	474944	5	0.495	-0.703	-0.790
0.39 – 0.43	507794	10	0.916	-0.088	-0.119
0.44 – 0.48	498221	13	1.210	0.191	0.204
0.49 – 0.54	472344	18	1.762	0.566	0.660
0.55 – 0.61	478466	9	0.876	-0.133	-0.169
0.62 – 0.79	471608	17	1.667	0.511	0.590
Slope curvature					
Concave (-21.534 – -0.001)	1206820	35	1.344	0.295	0.438
Flat (0 – 0.001)	1476204	16	0.510	-0.674	-0.967
Convex (0.002 – 27.276)	1173772	32	1.264	0.234	0.329
Distance to roads (m)					
0 - 18	468428	8	0.796	-0.228	-0.267
18.01 - 45	565044	17	1.393	0.332	0.390
45.01 - 81,01	560176	10	0.832	-0.184	-0.224
81.02 - 117.01	472655	14	1.372	0.316	0.358
117.02 - 171.01	476218	11	1.072	0.070	0.069
171.02 - 261.02	458687	10	1.013	0.013	0.003
261.03 - 477.04	435329	2	0.223	-1.501	-1.607
477.05 - 2,295.19	420259	11	1.214	0.194	0.209

ROC curve analysis was carried out on the weight of each landslide causative factor to obtain its influence on the landslide occurrence. The AUC value below 0.6 was supposed to have a low influence between a landslide factor to landslides [19], [34], [36]. The AUC values for all parameters in this study varied from 0.595 to 0.876 (TABLE II).

TABLE II
THE AUC VALUES OF ALL LANDSLIDE CAUSATIVE FACTORS

Parameter	AUC value
Slope (%)	0.876
Lithology	0.845
Rainfall	0.823
Elevation	0.821
Geomorphology	0.806
Aspect	0.787
River density	0.763
Distance to rivers	0.752
Road density	0.715
Vegetation index	0.637
PGA	0.613
Slope curvature	0.599
Distance to roads	0.595

Among all factors, five landslide factors have the greatest influence on the landslide occurrence, with the AUC values more than 0.8. Those factors are slope (0.876), lithology (0.845), rainfall (0.823), elevation (0.821), and geomorphology (0.806). The slope is the most influential factor to landslide in this study area. It has a strong relationship with shear stress. The increasing slope gradient generally causes increased shear stress and slope instability [7].

As shown in TABLE II, it can be seen that two parameters have AUC values less than 0.6, i.e., the slope curvature and the distance to the roads. Thus, two scenarios were conducted in LSM modeling to investigate the influence of the AUC values threshold on the landslide susceptibility model accuracy. The first scenario (scenario-1) considered only eleven factors that met the AUC threshold value. The second scenario (scenario-2) involved all the thirteen landslide causative parameters.

A. Scenario-1

The parameter selection in scenario-1 was determined by the threshold value of the AUC of higher than 0.6 [19], [34], [36]. Therefore, this scenario only used eleven parameters in the LSM modeling because two parameters, i.e., the distance to roads and the slope curvature, were omitted. The FR, IV, and WoE models of landslide susceptibility were validated by training and test data to obtain the success and predictive rates, respectively. Model validation is a mandatory step in any modeling to assess model performance. The success rate of FR, IV, and WoE was 0.911, 0.944, and 0.942. Meanwhile, the predictive rate was 0.901 for FR and 0.919 for both IV and WoE. Fig. 5 shows the ROC curves and AUC values for the success rate and the predictive rate of scenario-1.

B. Scenario-2

The scenario-2 used all parameters because it considered the importance of other parameters, namely slope curvature and distance to roads. In scenario-1, the distance to road variable was classified by the quantile classification method. Meanwhile, in scenario-2, the distance to road variable was classified by another classification method, namely manual classification. Accordingly, the AUC value of distance to roads increased from 0.595 to 0.616. The classes of distance to roads based on manual classification and the weight can be seen in TABLE III. This AUC value indicates that the manual classification method is more suitable for this variable than the quantile method. The manual classification method was also used for classifying the same factor by a previous LSM study [51].

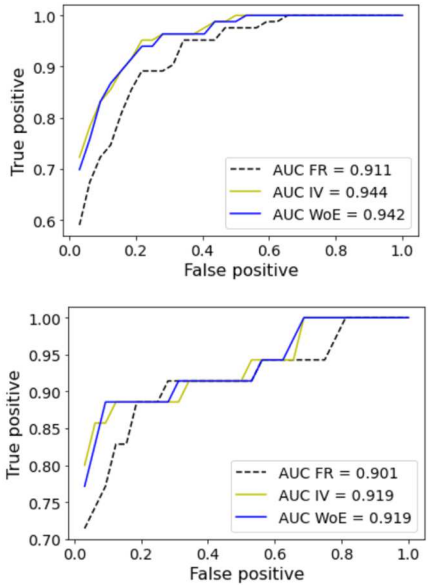

Fig. 5 ROC curves for the scenario-1: success rate (above) and predictive rate (bottom)

Similar to the LSM in scenario-1, the LSM in scenario-2, which involved all thirteen parameters, was validated. With the addition of those two factors, the model accuracy improved both for success and predictive rates. The success rates of FR, IV, and WoE were 0.923, 0.956, and 0.953, respectively. Meanwhile, the predictive rates of all models were 0.908, 0.927, and 0.923, respectively (Fig. 6).

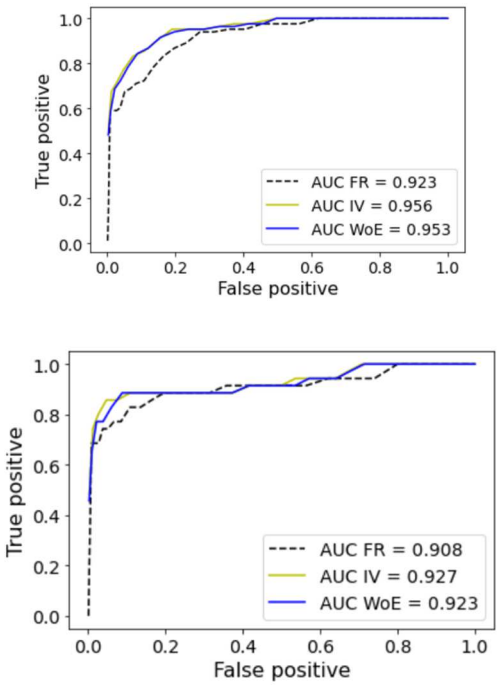

Fig. 6 ROC curves for the scenario-2: success rate (top) and predictive rate (bottom)

Thus, it is clear that the accuracy values of those three models were varied but are not much different. This result is consistent with some previous model comparative studies [21], [35]. As indicated in TABLE IV, the performance of those models in scenario-2 is better than those in scenario-1. Therefore, it can be concluded that eliminating specific landslide parameters with an AUC value below 0.6 can reduce the accuracy of the model.

TABLE III
THE SPATIAL RELATIONSHIP BETWEEN LANDSLIDES AND DISTANCE TO ROADS CLASSIFIED BY MANUAL CLASSIFICATION METHOD

Distance to roads (m)	Σ pixels	Σ landslide pixels	FR	IV	WoE
0 – 50	1082588	25	1.072	0.070	0.058
50.01 – 100	755366	13	0.802	-0.221	-0.308
100.01 – 200	885421	29	1.516	0.416	0.542
200.01 – 300	395473	5	0.592	-0.524	-0.610
300.01 – 500	343192	2	0.279	-1.279	-1.383
500.01 – 1,000	293346	5	0.795	-0.230	-0.287
1,000.01 – 1,500	77647	4	2.377	0.866	0.854
> 1,500.01	23763	0	0.012	-4.431	-4.478

TABLE IV
AUC VALUES OF ALL THREE MODELS IN SCENARIO-1 AND -2

Models	Scenario-1		Scenario-2	
	Success rate	Predictive rate	Success rate	Predictive rate
FR	0.911	0.901	0.923	0.908
IV	0.944	0.919	0.956	0.927
WoE	0.942	0.919	0.953	0.923

Table II shows that the distance to road variable was classified using the quantile method, producing the AUC value of 0.595. Meanwhile, by changing the classification method, the AUC value of distance to road variable increased to 0.616. Despite the low AUC value, the distance to road parameter is highly recommended to be involved in LSM modeling because road construction in mountainous areas disturbs the original force equilibrium in the slopes and increases the slope instability along the roads [11], [52]–[54]. Thus, parameters with a low AUC value should not immediately be omitted but must be further analyzed in connection to changes in classification methods or conditions in the field.

The AUC value of slope curvature is also less than 0.6 (TABLE II). However, concave and convex had high landslide probability indicated by FR weight of higher than 1, and the IV and WoE weights are positive (TABLE I). These results are also in line with previous studies, which stated that most landslides occur on convex and concave slopes [19], [37], [55].

The AUC value for slope curvature is less than 0.6 because this parameter was only classified into three classes, namely convex, flat, and concave, in this study. Similar classes of the slope curvature parameter were also used in other previous studies on landslide susceptibility [6], [35], [37]. However, a previous study that used nine classes of slope curvature produced an AUC value of higher than 0.6 [19].

Fig. 7 illustrates that the landslide probability of convex and concave slopes was almost equal, and some landslide occurrences were also found in the flat curvature. Thus, the landslide source area consisted of a nearly even mixture of three types of curvature. Although landslides occurred in the convex slope generally, in more detail, some landslide portions were in flat curvatures, as indicated by flat pixels in Fig. 7.

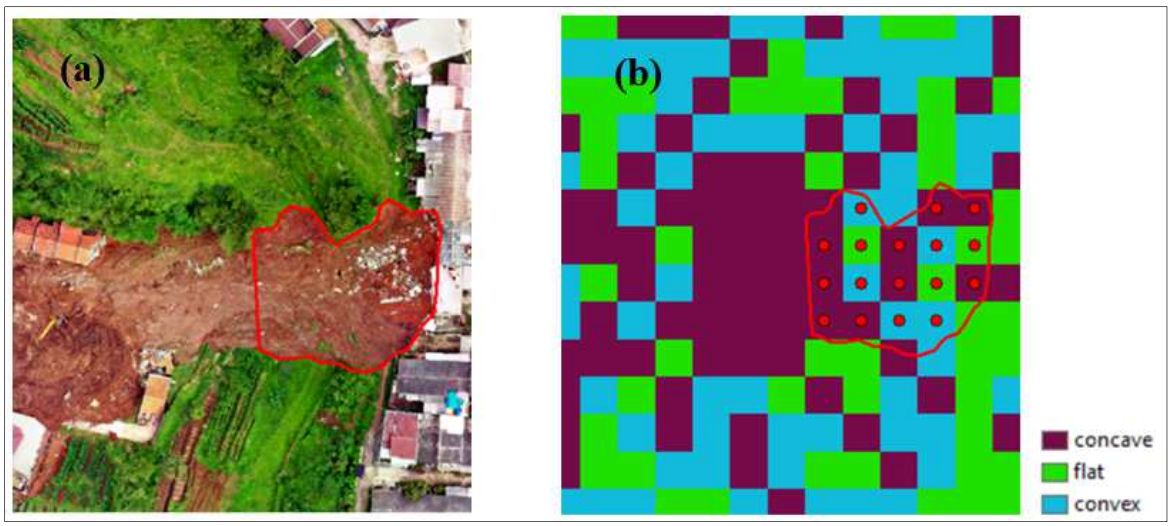

Fig. 7 The landslide source area of Cimanggung consisted of three types of curvature: (a) the UAV photos, (b) the slope curvature map

Landslide susceptibility zonation for the study area was generated from the LSM of scenario-2 that involved all thirteen parameters because this scenario has higher accuracy than scenario-1 (Fig. 8). The zonation is derived by classifying the landslide susceptibility index (LSI) qualitatively. It can be based on expert judgment or the related histogram [51]. In this study, each LSI from scenario-2 was split into five classes: very low (Class 1), low (Class 2), medium (Class 3), high (Class 4), and very high (Class 5) [20]. The very low class indicates the most stable zone, and the very high class shows the most unstable zone (TABLE V).

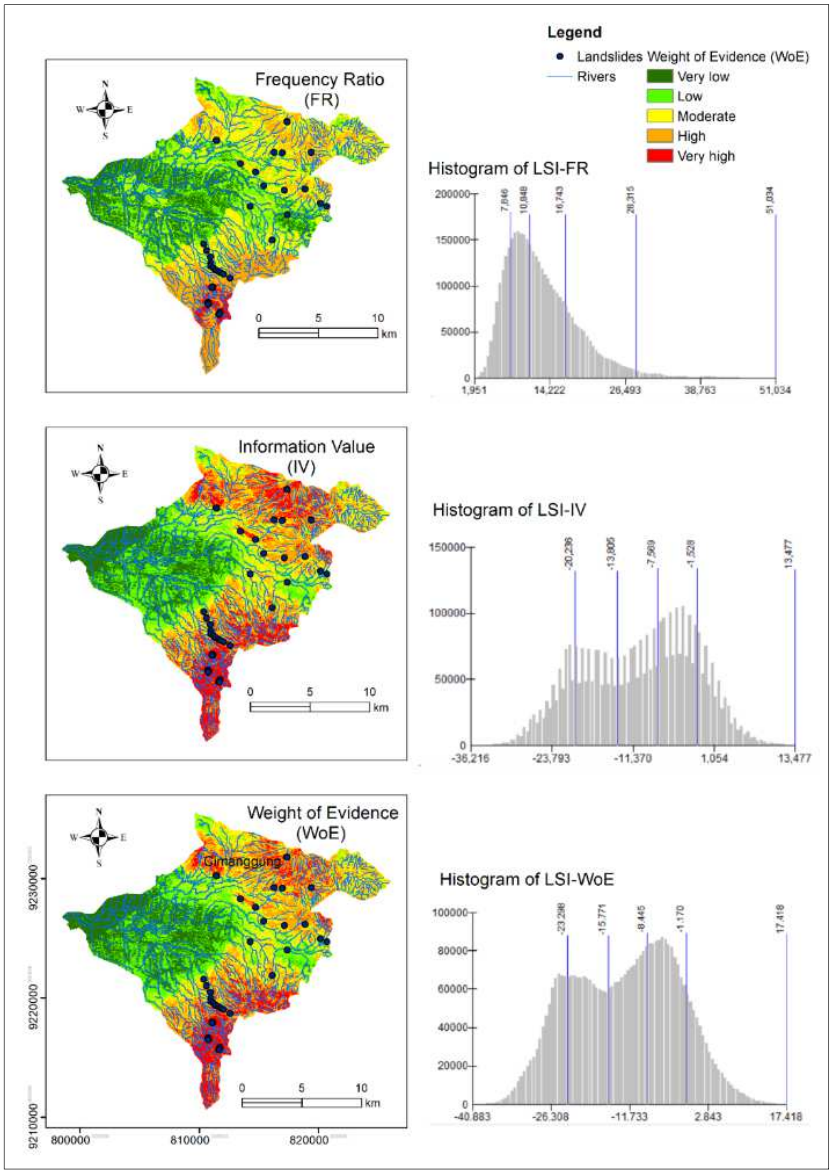

Fig. 8 The landslide susceptibility maps (LSMs) of FR, IV, and WoE

TABLE V
LANDSLIDE SUSCEPTIBILITY CLASS OF THE CITARIK SUB-WATERSHED

Class	LSI	Area		Landslides	
		Pixels	%	Pixels	%
FR					
1	1.951 – 7.846	715750	18.558	0	0
2	7.847 – 10.848	946454	24.540	5	4.237
3	10.849 – 16.743	1331574	34.525	8	6.780
4	16.744 – 28.315	781296	20.258	32	27.119
5	28.316 – 51.034	81722	2.119	73	61.864
IV					
1	-36.216 – -20.236	612945	15.893	0	0
2	-20.235 – -13.805	786284	20.387	2	1.695
3	-13.804 – -7.569	833679	21.616	3	2.542
4	-7.568 – -1.528	1006802	26.105	6	5.085
5	-1.527 – 13.477	617086	16.000	107	90.678
WoE					
1	-40.883 – -23.298	677476	17.566	0	0
2	-23.297 – -15.771	821763	21.307	2	1.695
3	-15.770 – -8.445	875391	22.697	4	3.390
4	-8.444 – -1.170	990282	25.676	9	7.627
5	-1.169 – 17.418	491884	12.754	103	87.288

LSI of frequency ratio (FR) has a data distribution of a positive skewness curve ranging from 1.951 to 51.034. Meanwhile, LSI of Information Value (IV) has a multi-modal distribution with a range value of -36.216 to 13.477, and WoE has a bimodal (double-peak) distribution with a range value of -40.883 to 17.418 (Fig. 8). Based on the data distribution, the LSI of FR was classified using geometrical intervals due to its skewness of the data distribution [51]. The classification method for LSI of IV and WoE was the natural break. The very low class (Class 1) indicated the stable zone; no landslide has occurred there, either in the map of FR, IV, or WoE. From TABLE V, it can be concluded that landslide occurrences were dominated in the very high class (Class 5) and decreased gradually to the lower classes.

Those three landslide susceptibility maps (LSMs) showed that northern, northeastern, south-eastern, and southern parts of the sub-watershed are under high to very high susceptibility to landslides, including the Cimanggung area, where a recent deadly double landslide occurred. The recent landslide is located in the high susceptibility zone on the LSM-FR and the very high susceptibility zone on the LSM-IV and LSM-WoE.

Therefore, it indicates that areas in the high and very high susceptibility zones of those three LSMs should be considered to be mitigated. The performance of those three models, both in scenario-1 and scenario-2, is excellent, with the AUC values more than 0.9, referring to the AUC value classification [38], [49].

IV. Conclusion

This study aims to evaluate the threshold of the area under curve (AUC) value for parameter selection in the landslide susceptibility mapping, with a case study of the Citarik sub-watershed. The performance of FR, IV, and WoE models in scenario-1 that used the selected eleven landslide parameters and scenario-2 that used all thirteen parameters is excellent, with an AUC value of more than 0.9. Regarding the threshold of AUC value in parameter selection, it can be concluded that eliminating specific landslide parameters with an AUC value below 0.6 can reduce the model's accuracy. The recent deadly landslide area is located in the high to very high landslide susceptibility zone based on the modeling results. Thus, detailed mapping is necessary to mitigate hazards in all landslide-prone areas, especially in residential areas.

Acknowledgment

The 2018 Saintek Scholarship Program of the Ministry of Research, Technology, and Higher Education of the Republic of Indonesia supports this study. The authors are grateful to the Department of Geomatics and Engineering and the Center for Remote Sensing–Bandung Institute of Technology (ITB) for their support. The authors are obliged to the Landslide Research Group of Research Center for Geotechnology-LIPI, the Geospatial Information Agency of Indonesia (BIG), Geological Agency of Indonesia, the European Space Agency (ESA), and the Center for Hydrometeorology and Remote Sensing (CHRS)–the University of California (UCI), for providing data for this study.

References

[1] D. Petley, "Protecting the rescuers – a disastrous double landslide at Cihanjuang in Indonesia and a lucky escape in Italy," 2021. https://blogs.agu.org/landslideblog/2021/01/10/cihanjuang/ (accessed Jan. 11, 2021).

[2] H. Hong et al., Landslide susceptibility assessment at the Wuning area, China: a comparison between multi-criteria decision making, bivariate statistical and machine learning methods, vol. 96, no. 1. Springer Netherlands, 2019.

[3] F. Li *et al.*, "Influence of earthquakes on landslide susceptibility in a seismic prone catchment in central Asia," *Appl. Sci.*, vol. 11, no. 9, 2021, doi: 10.3390/app11093768.

[4] C. J. van Westen, E. Castellanos, and S. L. Kuriakose, "Spatial data for landslide susceptibility, hazard, and vulnerability assessment: An overview," *Eng. Geol.*, vol. 102, no. 3–4, pp. 112–131, 2008, doi: 10.1016/j.enggeo.2008.03.010.

[5] J. I. Barredo, A. Benavides, J. Hervás, and C. J. Van Westen, "Comparing heuristic landslide hazard assessment techniques using GIS in the Tirajana basin, Gran Canaria Island, Spain," *Int. J. Appl. Earth Obs. Geoinf.*, vol. 2000, no. 1, pp. 9–23, 2000, doi: 10.1016/s0303-2434(00)85022-9.

[6] S. Lee and J. A. Talib, "Probabilistic landslide susceptibility and factor effect analysis," *Environ. Geol.*, vol. 47, no. 7, pp. 982–990, 2005, doi: 10.1007/s00254-005-1228-z.

[7] B. Pradhan, "Landslide susceptibility mapping of a catchment area using frequency ratio, fuzzy logic and multivariate logistic regression approaches," *J. Indian Soc. Remote Sens.*, vol. 38, no. 2, pp. 301–320, 2010, doi: 10.1007/s12524-010-0020-z.

[8] W. Luo and C. C. Liu, "Innovative landslide susceptibility mapping supported by geomorphon and geographical detector methods," *Landslides*, vol. 15, no. 3, pp. 465–474, 2018, doi: 10.1007/s10346-017-0893-9.

[9] M. S. G. Adnan, M. S. Rahman, N. Ahmed, B. Ahmed, M. F. Rabbi, and R. M. Rahman, "Improving spatial agreement in machine learning-based landslide susceptibility mapping," *Remote Sens.*, vol. 12, no. 20, pp. 1–23, 2020, doi: 10.3390/rs12203347.

[10] V. H. Nhu *et al.*, "Landslide susceptibility mapping using machine learning algorithms and remote sensing data in a tropical environment," *Int. J. Environ. Res. Public Health*, vol. 17, no. 14, pp. 1–23, 2020, doi: 10.3390/ijerph17144933.

[11] X. Zhou *et al.*, "Zonation of Landslide Susceptibility in Ruijin , Jiangxi , China," 2021.

[12] M. Juliev, M. Mergili, I. Mondal, B. Nurtaev, A. Pulatov, and J. Hübl, "Comparative analysis of statistical methods for landslide susceptibility mapping in the Bostanlik District, Uzbekistan," *Sci. Total Environ.*, vol. 653, pp. 801–814, 2019, doi: 10.1016/j.scitotenv.2018.10.431.

[13] H. J. Oh, S. Lee, and G. M. Soedradjat, "Quantitative landslide susceptibility mapping at Pemalang area, Indonesia," *Environ. Earth Sci.*, vol. 60, no. 6, pp. 1317–1328, 2010, doi: 10.1007/s12665-009-0272-5.

[14] R. Mind'je *et al.*, "Landslide susceptibility and influencing factors analysis in Rwanda," *Environ. Dev. Sustain.*, vol. 22, no. 8, pp. 7985–8012, 2020, doi: 10.1007/s10668-019-00557-4.

[15] S. Razavizadeh, K. Solaimani, M. Massironi, and A. Kavian, "Mapping landslide susceptibility with frequency ratio, statistical index, and weights of evidence models: a case study in northern Iran," *Environ. Earth Sci.*, vol. 76, no. 14, pp. 1–16, 2017, doi: 10.1007/s12665-017-6839-7.

[16] Y. Ge *et al.*, "A comparison of five methods in landslide susceptibility assessment: a case study from the 330-kV transmission line in Gansu Region, China," *Environ. Earth Sci.*, vol. 77, no. 19, pp. 1–15, 2018, doi: 10.1007/s12665-018-7814-7.

[17] A. A. Othman, R. Gloaguen, L. Andreani, and M. Rahnama, "Improving landslide susceptibility mapping using morphometric features in the Mawat area, Kurdistan Region, NE Iraq: Comparison of different statistical models," *Geomorphology*, vol. 319, pp. 147–160, 2018, doi: 10.1016/j.geomorph.2018.07.018.

[18] J. Liu and Z. Duan, "Quantitative assessment of landslide susceptibility comparing statistical index, index of entropy, and weights of evidence in the Shangnan Area, China," *Entropy*, vol. 20, no. 11, pp. 9–11, 2018, doi: 10.3390/e20110868.

[19] S. Sumaryono, D. Muslim, N. Sulaksana, and Y. Dasatriana, "Weights of Evidence Method for Landslide Susceptibility Mapping in Tandikek and Damar Bancah, West Sumatra, Indonesia," *Int. J. Sci. Res.*, vol. 4, no. 10, pp. 1283–1290, 2015.

[20] A. K. Batar and T. Watanabe, "Landslide Susceptibility Mapping and Assessment Using Geospatial Platforms and Weights of Evidence (WoE) Method in the Indian Himalayan Region: Recent Developments, Gaps, and Future Directions," *ISPRS Int. J. Geo-Information*, vol. 10, no. 3, p. 114, 2021, doi: 10.3390/ijgi10030114.

[21] A. Aditian, T. Kubota, and Y. Shinohara, "Comparison of GIS-based landslide susceptibility models using frequency ratio, logistic regression, and artificial neural network in a tertiary region of Ambon, Indonesia," *Geomorphology*, vol. 318, pp. 101–111, 2018, doi: 10.1016/j.geomorph.2018.06.006.

[22] E. R. Sujatha and V. Sridhar, "Landslide susceptibility analysis: A logistic regression model case study in Coonoor, India," *Hydrology*, vol. 8, no. 1, 2021, doi: 10.3390/hydrology8010041.

[23] U. Ozturk, M. Pittore, R. Behling, S. Roessner, L. Andreani, and O. Korup, "How robust are landslide susceptibility estimates?," *Landslides*, vol. 18, no. 2, pp. 681–695, 2021, doi: 10.1007/s10346-020-01485-5.

[24] B. Kalantar, B. Pradhan, S. Amir Naghibi, A. Motevalli, and S. Mansor, "Assessment of the effects of training data selection on the landslide susceptibility mapping: a comparison between support vector machine (SVM), logistic regression (LR) and artificial neural networks (ANN)," *Geomatics, Nat. Hazards Risk*, vol. 9, no. 1, pp. 49–69, 2018, doi: 10.1080/19475705.2017.1407368.

[25] T. Kavzoglu, I. Colkesen, and E. K. Sahin, *Landslides: Theory, Practice and Modelling*, vol. 50. 2019.

[26] M. Marjanovic, "Advanced methods for landslide assessment using GIS," Palacký University Olomouc, 2013.

[27] W. Chen, H. R. Pourghasemi, and S. A. Naghibi, "Prioritization of landslide conditioning factors and its spatial modeling in Shangnan

County, China using GIS-based data mining algorithms," *Bull. Eng. Geol. Environ.*, vol. 77, no. 2, pp. 611–629, 2018, doi: 10.1007/s10064-017-1004-9.
[28] J. Cao, Z. Zhang, C. Wang, J. Liu, and L. Zhang, "Susceptibility assessment of landslides triggered by earthquakes in the Western Sichuan Plateau," *Catena*, vol. 175, no. December 2018, pp. 63–76, 2019, doi: 10.1016/j.catena.2018.12.013.
[29] J. S. Lai and F. Tsai, "Improving GIS-based landslide susceptibility assessments with multi-temporal remote sensing and machine learning," *Sensors (Switzerland)*, vol. 19, no. 17, pp. 1–25, 2019, doi: 10.3390/s19173717.
[30] P. Reichenbach, M. Rossi, B. D. Malamud, M. Mihir, and F. Guzzetti, "A review of statistically-based landslide susceptibility models," *Earth-Science Rev.*, vol. 180, no. March, pp. 60–91, 2018, doi: 10.1016/j.earscirev.2018.03.001.
[31] Y. Arifianti, Pamela, F. Agustin, and D. Muslim, "Comparative study among bivariate statistical models in landslide susceptibility map," *Indones. J. Geosci.*, vol. 7, no. 1, pp. 51–63, 2020, doi: 10.17014/IJOG.7.1.51-63.
[32] T. Blaschke, B. Feizizadeh, and D. Hölbling, "Object-based image analysis and digital terrain analysis for locating landslides in the Urmia Lake basin, Iran," *IEEE J. Sel. Top. Appl. Earth Obs. Remote Sens.*, vol. 7, no. 12, pp. 4806–4817, 2014, doi: 10.1109/JSTARS.2014.2350036.
[33] C. Xu, "Preparation of earthquake-triggered landslide inventory maps using remote sensing and GIS technologies: Principles and case studies," *Geosci. Front.*, vol. 6, no. 6, pp. 825–836, 2015, doi: 10.1016/j.gsf.2014.03.004.
[34] Y. Arifianti and F. Agustin, *GIS Landslide*. Tokyo: Springer Japan, 2017.
[35] E. Nohani, M. Moharrami, and S. Sharafi, "Landslide Susceptibility Mapping Using Different GIS-Based Bivariate Models," *Water*, vol. 11, no. 1402, pp. 1–22, 2019.
[36] Pamela, I. A. Sadisun, and Y. Arifianti, "Weights of Evidence Method for Landslide Susceptibility Mapping in Takengon, Central Aceh, Indonesia," *IOP Conf. Ser. Earth Environ. Sci.*, vol. 118, no. 1, 2018, doi: 10.1088/1755-1315/118/1/012037.
[37] S. Mandal and K. Mandal, "Bivariate statistical index for landslide susceptibility mapping in the Rorachu river basin of eastern Sikkim Himalaya, India," *Spat. Inf. Res.*, vol. 26, no. 1, pp. 59–75, 2018, doi: 10.1007/s41324-017-0156-9.
[38] H. R. Pourghasemi, H. R. Moradi, and S. M. Fatemi Aghda, "Landslide susceptibility mapping by binary logistic regression, analytical hierarchy process, and statistical index models and assessment of their performances," *Nat. Hazards*, vol. 69, no. 1, pp. 749–779, 2013, doi: 10.1007/s11069-013-0728-5.
[39] D. Wang, M. Hao, S. Chen, Z. Meng, D. Jiang, and F. Ding, "Assessment of landslide susceptibility and risk factors in China," *Nat. Hazards*, no. 0123456789, 2021, doi: 10.1007/s11069-021-04812-8.
[40] R. Schlögel, I. Marchesini, M. Alvioli, P. Reichenbach, M. Rossi, and J. P. Malet, "Optimizing landslide susceptibility zonation: Effects of DEM spatial resolution and slope unit delineation on logistic regression models," *Geomorphology*, vol. 301, pp. 10–20, 2018, doi: 10.1016/j.geomorph.2017.10.018.
[41] B. T. Pham *et al.*, "Landslide susceptibility assessment by novel hybrid machine learning algorithms," *Sustain.*, vol. 11, no. 16, pp. 1–25, 2019, doi: 10.3390/su11164386.
[42] J. Cao, Z. Zhang, J. Du, L. Zhang, Y. Song, and G. Sun, "Multi-geohazards susceptibility mapping based on machine learning—a case study in Jiuzhaigou, China," *Nat. Hazards*, vol. 102, no. 3, pp. 851–871, 2020, doi: 10.1007/s11069-020-03927-8.
[43] D. Noor, *Geomorfologi*. Universitas Pakuan, 2010.
[44] A. K. S. D. P. Budha, "GIS Based Landslide Susceptibility Mapping along the Road Section from Bandeu to Barahabise, Sindhupal Chowk District of Nepal," *Int. J. Sci. Res.*, vol. 7, no. 11, pp. 465–471, 2018, doi: 10.21275/ART20192474.
[45] E. Pimiento, "Shallow Landslide Susceptibility Modelling and Validation," Ehime University (Japan), 2010.
[46] H. He, D. Hu, Q. Sun, L. Zhu, and Y. Liu, "A landslide susceptibility assessment method based on GIS technology and an AHP-weighted information content method: A case study of southern Anhui, China," *ISPRS Int. J. Geo-Information*, vol. 8, no. 6, 2019, doi: 10.3390/ijgi8060266.
[47] S. Beguería, "Validation and evaluation of predictive models in hazard assessment and risk management," *Nat. Hazards*, vol. 37, no. 3, pp. 315–329, 2006, doi: 10.1007/s11069-005-5182-6.
[48] I. Yilmaz, "Landslide susceptibility mapping using frequency ratio, logistic regression, artificial neural networks and their comparison: A case study from Kat landslides (Tokat-Turkey)," *Comput. Geosci.*, vol. 35, no. 6, pp. 1125–1138, 2009, doi: 10.1016/j.cageo.2008.08.007.
[49] A. Merghadi, B. Abderrahmane, and D. Tien Bui, "Landslide susceptibility assessment at Mila basin (Algeria): A comparative assessment of prediction capability of advanced machine learning methods," *ISPRS Int. J. Geo-Information*, vol. 7, no. 7, 2018, doi: 10.3390/ijgi7070268.
[50] A. R. Rasyid, N. P. Bhandary, and R. Yatabe, "Performance of frequency ratio and logistic regression model in creating GIS based landslides susceptibility map at Lompobattang Mountain, Indonesia," *Geoenvironmental Disasters*, vol. 3, no. 1, 2016, doi: 10.1186/s40677-016-0053-x.
[51] G. Samodra, G. Chen, J. Sartohadi, and K. Kasama, "Comparing data-driven landslide susceptibility models based on participatory landslide inventory mapping in Purwosari area, Yogyakarta, Java," *Environ. Earth Sci.*, vol. 76, no. 4, pp. 1–19, 2017, doi: 10.1007/s12665-017-6475-2.
[52] M. M. Awawdeh, M. A. ElMughrabi, and M. Y. Atallah, "Landslide susceptibility mapping using GIS and weighted overlay method: a case study from North Jordan," *Environ. Earth Sci.*, vol. 77, no. 21, pp. 1–15, 2018, doi: 10.1007/s12665-018-7910-8.
[53] E. Psomiadis, A. Papazachariou, K. X. Soulis, D. S. Alexiou, and I. Charalampopoulos, "Landslide mapping and susceptibility assessment using geospatial analysis and earth observation data," *Land*, vol. 9, no. 5, 2020, doi: 10.3390/LAND9050133.
[54] W. Xie *et al.*, "A Novel Hybrid Method for Landslide Susceptibility Mapping-Based GeoDetector and Machine Learning Cluster : A Case of Xiaojin County , China," 2021.
[55] Z. Umar, B. Pradhan, A. Ahmad, M. N. Jebur, and M. S. Tehrany, "Earthquake induced landslide susceptibility mapping using an integrated ensemble frequency ratio and logistic regression models in West Sumatera Province, Indonesia," *Catena*, vol. 118, no. September 2009, pp. 124–135, 2014, doi: 10.1016/j.catena.2014.02.005.